Ferroelectricity in the guanidinium compound $[C(NH_2)_3]_4Cl_2SO_4$: Synthesis and characterization

Marek Szafrański
Institute of Physics, Adam Mickiewicz University, Umultowska 85, 61-614 Poznań, Poland
(Received 26 April 2005; published 24 August 2005)

A guanidinium compound, $[C(NH_2)_3]_4Cl_2SO_4$, has been synthesized and characterized by x-ray diffraction, calorimetric, dilatometric, and dielectric measurements, and by optical examination in polarized light. At room temperature the initial crystal structure is orthorhombic, space group $Cmc2_1$, and it exhibits ferroelectric order. The crystal is built of two anionic sublattices with different ion valency, and guanidinium cations, which occupy three crystallographically different sites. On heating the crystal undergoes two first-order phase transitions: at $T_1=352$ K to the intermediate orthorhombic phase II, and at $T_C=356$ K to the paraelectric tetragonal phase I, space group $I\bar{4}2m$. The structure of the paraelectric phase is highly disordered and the prevailing part of this disorder persists in the crystal lattice after the reverse transition. Thus, at first the crystal transforms from the tetragonal phase to the disordered low-symmetry ferroelectric phase IV, which is metastable, and than slowly crystallizes to the initial, ordered phase III. Despite the prominent order-disorder contribution to the transition mechanism the ferroelectric polarization in $[C(NH_2)_3]_4Cl_2SO_4$ is of displacive-type.

DOI: 10.1103/PhysRevB.72.054122 PACS number(s): 77.80.−e, 61.50.Ks, 77.22.−d, 65.40.−b

I. INTRODUCTION

The discovery of ferroelectric properties in guanidinium aluminum sulfate hexahydrate,[1] $C(NH_2)_3Al(SO_4)_2\times 6H_2O$ (GASH), has aroused a wide interest in guanidinium compounds. The guanidinium cation $[C(NH_2)_3]^+$ (hereafter G) belongs to the simplest organic chemical units, but exhibits certain peculiar features, which play a prominent role for the properties of solids. This cation is characterized by a relatively small ionic radius, planar conformation, and high symmetry[2] (D_{3h} in a free state), and it is also a potential H-donor in hydrogen bonds. As has recently been demonstrated these features can be employed for engineering functional molecular materials.[3–5] Intense studies in this field have brought about, among others, a novel class of nanoporous crystals.[4] These layered materials with adjustable porosity are based on two-dimensional H-bonded sheets composed of guanidinium cations and the sulfonate groups of organosulfonate anions. The same structural motifs, characterized by the quasihexagonal patterns of NH···O hydrogen bonds linking the ions, are formed in the structures of guanidinium perchlorate[6] and guanidinium nitrate.[7,8] Both these crystals undergo structural phase transitions. The first-order phase transition in guanidinium nitrate is especially noteworthy since it is accompanied by a record shear strain visible in a form of nearly 45% deformation of the crystal.[9] Moreover, in this substance the temperature-induced H-site centering in the medium-strength heteronuclear hydrogen bonds has been evidenced.[10] Thus hydrogen bonds have been shown to be responsible for the structure and properties of all these materials. But on the other hand, there are the structures of guanidinium salts with a minor role of the hydrogen-bonding interaction. The best example is diguanidinium tetraiodoplumbate, the large-gap semiconductor showing a very unusual pressure-temperature phase diagram.[11] Among the numerous transformable guanidinium compounds there are also crystals undergoing ferroelastic phase transitions,[11–13] transitions associated with thermochromic effect,[14] and others, but as far as we know, ferroelectric properties have been observed exclusively in GASH and the several isomorphous sulfates and selenates.[15] All the members from the GASH group are ferroelectrics at room temperature and they occupy a special position in the ferroelectric family owing to the absence of the ferroelectric-paraelectric phase transitions.

In this paper we describe the structure and basic properties of tetraguanidinium dichloro-sulfate, $G_4Cl_2SO_4$. This compound is formed from a 2:1 stoichiometric mixture of two simple guanidinium salts: GCl and G_2SO_4. While the substrates do not undergo phase transitions and do not have polar properties,[16–19] the newly obtained crystal structure exhibits ferroelectric order in a wide temperature range, including room temperature.

II. EXPERIMENT

$G_4Cl_2SO_4$ was synthesized by dissolving GCl and G_2SO_4 in molar ratio 2:1 in water. The substance obtained after evaporation of the solvent was purified by threefold recrystallization from water solution. Colorless and transparent single crystals were grown by a slow evaporation method at room temperature. Calorimetric measurements were carried out by differential thermal analysis (DTA) using a homemade apparatus. The DTA experiments were performed on heating/cooling the samples at a rate of 3 K/min. The samples were prepared from single crystals ground into a fine powder. Oriented crystal plates with silver painted electrodes were used for dielectric studies. Measurements of complex electric permittivity as a function of temperature were carried out in the frequency range from 1 kHz to 13 MHz with a Hewlett-Packard 4192A impedance analyzer. The amplitude of the ac measuring electric field did not exceed 2 V/cm. The temperature of the samples was changed at a rate of 0.3 K/min in the vicinity of the phase transitions and 0.5 K/min elsewhere. The dielectric hysteresis loops were recorded by a Diamant-Drenck-Pepinsky bridge method[20] at a frequency of 50 Hz. The temperature

TABLE I. Crystal data and structure refinement information for $G_4Cl_2SO_4$ at 298, 345, and 360 K.

Temperature (K)	298	345	360
Crystal size (mm)	$0.42\times0.40\times0.38$	$0.5\times0.2\times0.2$	$0.45\times0.32\times0.3$
Space group	$Cmc2_1$	$Cmc2_1$	$I\bar{4}2m$
Unit-cell dimensions (Å)	$a=14.213(3)$	$a=14.263(6)$	$a=10.138(5)$
	$b=9.474(5)$	$b=9.473(2)$	$c=9.493(2)$
	$c=14.414(4)$	$c=14.442(11)$	
Unit-cell volume (Å^3)	1940.9(12)	1951.3(17)	975.7(7)
Z/calculated density (Mg/m^3)	4/1.394	4/1.386	2/1.386
Absorption coefficient (mm^{-1})	0.477	0.474	0.474
θ range for data collection (°)	2.58–26.07	2.58–27.05	2.84–25.08
Reflections collected/unique	1925/1925	2116/2116	977/475(R_{int}=0.0284)
Data/restrains/parameters	1925/1/116	2116/1/116	475/0/54
Goodness-of-fit on F^2	1.133	1.011	1.071
Final R indices [$I>2\sigma(I)$]	$R1=0.028$, $wR2=0.0794$	$R1=0.0303$, $wR2=0.0793$	$R1=0.0366$, $wR2=0.097$
R indices (all data)	$R1=0.047$, $wR2=0.0949$	$R1=0.0912$, $wR2=0.0910$	$R1=0.065$, $wR2=0.1077$
Extinction coefficient	0.0149(12)	0.0005(5)	0.000(5)
Largest diff. peak and hole (eÅ^{-3})	0.185 and −0.249	0.162 and −0.235	0.181 and −0.208

dependence of spontaneous polarization was determined by a pyroelectric charge method using a Keithley 6514 electrometer.

The optical examinations of the $G_4Cl_2SO_4$ crystals were carried out with a polarizing microscope Eclipse E600 POL (Nikon) equipped with a Bertrand lens and Linkam cooling/heating stage THMSE 600.

The x-ray diffraction data sets were collected on a KM-4 diffractometer equipped with graphite monochromated Mo $K\alpha$ radiation. The θ-2θ scan mode at variable rate, depending on the reflection intensity, was applied. The intensities were corrected for Lorentz and polarization effects. The unit-cell dimensions were measured as a function of temperature by least-squares fits to 33 automatically centered reflections at fixed temperatures. The crystal was cooled/heated with a nitrogen stream using an Oxford Cryosystem device, the temperature was stabilized within 0.1 K.

The crystal structures were solved by direct methods with the SHELXS97 program[21] and refined by a full-matrix least-squares method on all F^2 data using the SHELXL97 program.[22] All the heavy atoms were refined with anisotropic temperature factors. The H-atoms were located from the molecular geometry and their isotropic temperature factors U_{iso} were assumed as 1.2 times U_{eq} of their closest heavy atoms. The crystal data together with experimental and refinement details are given in Table I. The final atomic coordinates and equivalent temperature factors are listed in Table II.

III. RESULTS

A. Calorimetric measurements

Figure 1 shows the result of calorimetric measurements performed on the polycrystalline $G_4Cl_2SO_4$ sample. Evident differences in the magnitude of thermal effects between the heating and cooling runs are clearly seen. The huge anomaly recorded on the first heating of the virgin sample is very broad and its shape suggests the presence of two overlapping peaks. Thus a sequence of phase transitions can be expected in the temperature range between 350 and 380 K. The total transition enthalpy ΔH^h derived from the peak area amounts to 13.5 kJ/mol, which corresponds to the entropy change $\Delta S^h=37.6$ J mol^{-1} K^{-1}. The value of ΔS^h is close to R ln 92 (R denotes a gas constant), which indicates an extremely high degree of disordering of the crystal structure in the high-temperature phase. Therefore, the behavior of the substance on the cooling run was unexpected. As illustrated in Fig. 1, a sharp single peak occurred at 352 K, but with the amplitude and area much reduced when compared to those in the first heating scan. The enthalpy of the reverse transition $\Delta H^c=2.54$ kJ/mol is about 5 times lower than ΔH^h and corresponds to the entropy change $\Delta S^c=7.26$ J mol^{-1} K^{-1} (R ln 2.4). The measurements in a wider temperature range, up to 120 K, did not reveal any additional thermal anomaly. Moreover, in a subsequent heating run only a single, small peak at 355 K was observed. We conclude from these measurements that the $G_4Cl_2SO_4$ crystals undergo a different sequence of phase transitions on the first heating and cooling cycles, and furthermore the prevailing part of the entropy gain in the high-temperature phase is retained by the crystal lattice after the reverse transition to the low-temperature phase. To clarify this unusual behavior of the crystal, a series of time-dependent calorimetric experiments has been performed. In these measurements, subsequent heating-cooling cycles were separated by the time periods from several to several hundred hours and the peak area in the heating scans was carefully monitored. Between the cycles the sample was kept at room temperature. The representative DTA runs are plotted in Fig. 2(a), while in Fig. 2(b) the time evolution of the thermal anomaly is shown. It is apparent that the anomaly grows gradually when the time period between the measurements increases. The restoration of the crystal low-entropy state requires about 2 weeks.

TABLE II. Atomic coordinates and equivalent isotropic displacement parameters (Å^2) for $G_4Cl_2SO_4$ at 298, 345, and 360 K.

	x	y	z	U_{eq}
		298 K		
Cl	0.7542(1)	0.7540(1)	0.5763(1)	0.058(1)
S	0.5	0.7441(1)	0.8078(1)	0.029(1)
O(1)	0.5	0.6595(2)	0.8933(2)	0.044(1)
O(2)	0.5839(1)	0.7115(2)	0.7528(1)	0.044(1)
O(3)	0.5	0.8951(2)	0.8311(2)	0.051(1)
C(1)	0.8029(2)	0.9045(2)	0.8396(2)	0.043(1)
N(11)	0.8472(2)	0.9609(3)	0.9107(2)	0.055(1)
N(12)	0.7429(2)	0.8015(3)	0.8537(2)	0.064(1)
N(13)	0.8182(2)	0.9506(3)	0.7552(2)	0.059(1)
C(2)	0.5	0.8731(4)	0.5063(2)	0.044(1)
N(21)	0.5802(2)	0.9225(3)	0.4722(2)	0.058(1)
N(22)	0.5	0.7770(4)	0.5712(3)	0.059(1)
C(3)	0.5	0.8604(4)	0.1596(2)	0.046(1)
N(31)	0.5796(2)	0.9083(3)	0.1934(2)	0.060(1)
N(32)	0.5	0.7652(4)	0.0926(3)	0.070(1)
		345 K		
Cl	0.7539(1)	0.7539(1)	0.5760(1)	0.069(1)
S	0.5	0.7451(1)	0.8082(1)	0.036(1)
O(1)	0.5	0.6611(3)	0.8933(2)	0.054(1)
O(2)	0.5833(1)	0.7127(2)	0.7532(1)	0.054(1)
O(3)	0.5	0.8951(3)	0.8319(2)	0.062(1)
C(1)	0.8034(2)	0.9060(3)	0.8386(2)	0.049(1)
N(11)	0.8469(2)	0.9620(3)	0.9099(2)	0.065(1)
N(12)	0.7429(2)	0.8040(3)	0.8529(2)	0.077(1)
N(13)	0.8184(2)	0.9522(3)	0.7547(2)	0.071(1)
C(2)	0.5	0.8715(5)	0.5054(3)	0.052(1)
N(21)	0.5804(2)	0.9201(3)	0.4722(2)	0.068(1)
N(22)	0.5	0.7760(4)	0.5706(3)	0.072(1)
C(3)	0.5	0.8595(5)	0.1594(3)	0.056(1)
N(31)	0.5787(2)	0.9080(3)	0.1930(2)	0.071(1)
N(32)	0.5	0.7644(5)	0.0927(4)	0.083(1)
		360 K		
Cl	1.0	0.5	0	0.091(1)
S	0.5	0.5	0	0.068(1)
O(1)	0.4790(14)	0.5210(14)	0.1370(20)	0.092(14)
O(2)	0.5665(14)	0.4335(14)	0.1090(30)	0.099(4)
O(3)	0.4780(40)	0.3550(30)	0.0480(50)	0.080(10)
O(4)	0.5	0.3460(20)	0	0.101(16)
C	0.8147(3)	0.1853(3)	0.1421(5)	0.081(1)
N(1)	0.7663(3)	0.0778(3)	0.1938(4)	0.112(1)
N(2)	0.7557(3)	0.2443(3)	0.0353(6)	0.134(2)

B. Temperature dependence of lattice parameters

Several attempts have been made to measure the temperature dependence of the lattice parameters of $G_4Cl_2SO_4$ in the vicinity of the phase transitions, on the first heating of the crystal. As a rule a coexistence of phases between 350 and 360 K hindered the measurements, but for selected crystals two distinct singularities in this temperature range have been observed in the temperature dependence of the unit-cell dimensions, as shown in Fig. 3. The results of these dilatometric studies evidence that $G_4Cl_2SO_4$ undergoes a sequence of

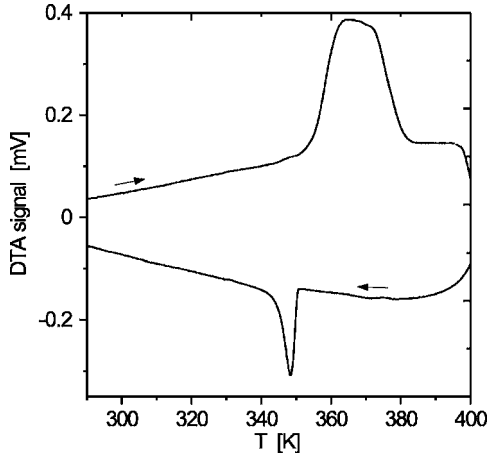

FIG. 1. DTA heating and cooling runs measured for the polycrystalline, virgin $G_4Cl_2SO_4$ sample.

two successive phase transitions. The clearly discontinuous changes at $T_1=352$ K and $T_2=356$ K indicate the first-order character of both transitions. Henceforth in this paper the room-temperature phase of the virgin $G_4Cl_2SO_4$ crystals will

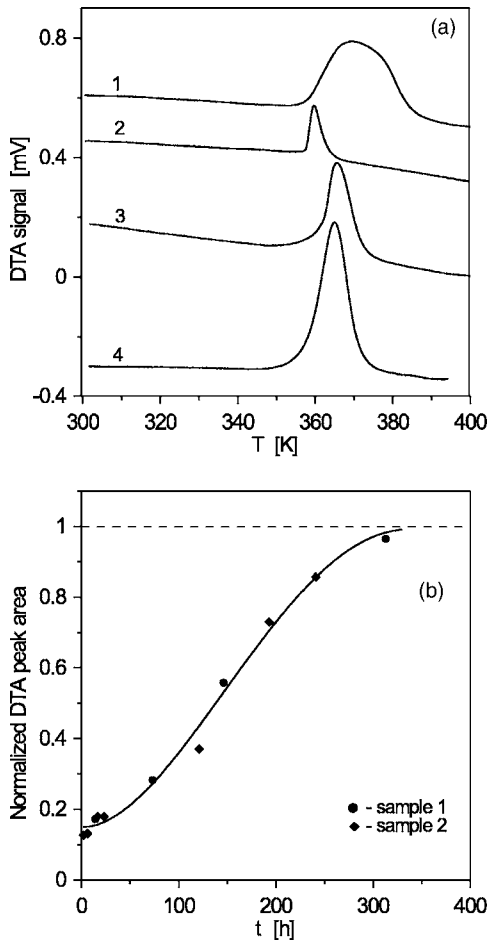

FIG. 2. Time evolution of the thermal anomaly in $G_4Cl_2SO_4$: (a) DTA first heating run–1, and subsequent runs after 1 h–2, 6 days–3, and 13 days–4 and (b) peak area as a function of the period of time between the subsequent measurements.

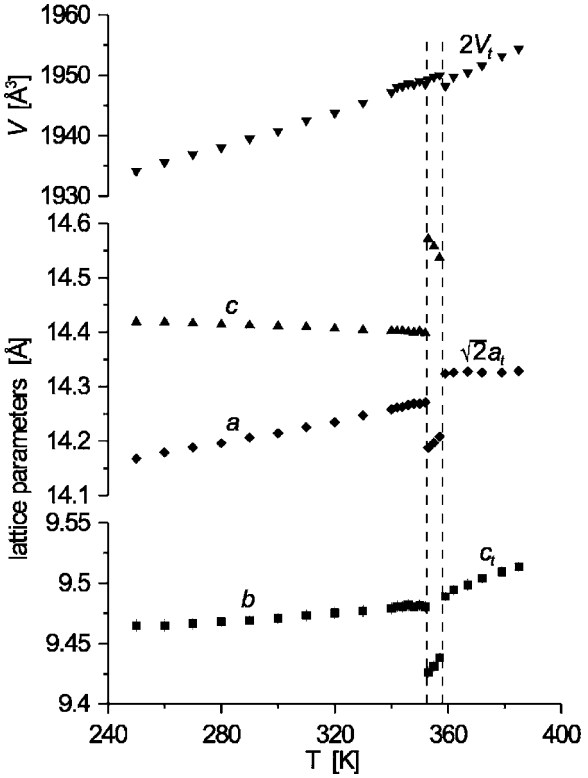

FIG. 3. Temperature dependence of the lattice parameters and unit-cell volume.

be referred to as III, the intermediate phase as II, and the high-temperature phase as I. At the transition temperature T_1 the changes in the crystal lattice dimensions are very distinct, but the orthorhombic unit-cell is preserved in the intermediate phase II. The abrupt increase in c is compensated by the shortening of a and b, so the volume change, which should occur at the first-order phase transition, is probably very small, below the accuracy of our measurements. It is worth noticing that thermal expansion of the crystal along the main crystallographic directions is the highest in the intermediate phase II, but it is not reflected in the temperature dependence of the unit-cell volume due to the compensation effect. The transition at T_2 is also associated with profound changes in the unit-cell dimensions as the crystal lattice loses its orthorhombic distortion and becomes tetragonal (see Fig. 3). It is interesting that the change in the crystal volume at T_2 is negative.

The change in the crystal symmetry was verified by optical examinations in polarized light. The crystal plate was oriented approximately perpendicular to the [010] direction of the orthorhombic phase III and the conoscopic pattern of the sample was observed during the heating from 300 to 400 K. As clearly seen in Fig. 4, the conoscopic pattern of $G_4Cl_2SO_4$ in phase III is typical of biaxial crystals, while after the transition to the phase I the crystal becomes optically uniaxial, consistent with the symmetry change from orthorhombic to tetragonal.

C. Crystal structure

In the phase III the structure of $G_4Cl_2SO_4$ is orthorhombic, space group $Cmc2_1$. The crystal is built of two anionic

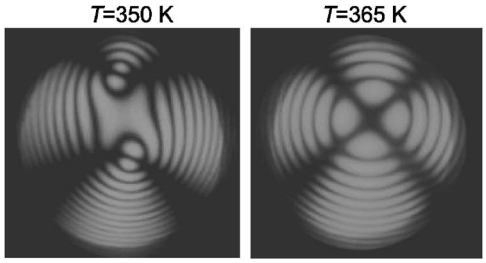

FIG. 4. Conoscopic patterns of the $G_4Cl_2SO_4$ crystal in the ferroelectric phase III at 350 K and in the paraelectric phase I at 365 K.

sublattices of monovalent Cl^- and divalent SO_4^{2-} anions, and guanidinium cations, as shown in Fig. 5(a). Therefore it should probably be more appropriate to write the crystal formula in the form $G_2SO_4 \times 2GCl$. The chlorine ions are located in general positions, while the SO_4^{2-} groups occupy special positions. The S, O(1), and O(3) atoms of the tetrahedron lie on the mirror-symmetry plane, which implies C_s symmetry of the SO_4^{2-} group. There are three crystallographically different guanidinium ions in the structure: $G(1)$ (the numbering of the cations is consistent with the labels of the carbon atoms in Table II) in a general site, and $G(2)$ and $G(3)$ in special sites—both with their carbon atoms and one of the nitrogens located on the symmetry planes. Apart from electrostatic forces the cations and anions are tied by a three-dimensional system of hydrogen bonds. Each chlorine is connected to the neighboring guanidinium cations by seven NH···Cl hydrogen bonds. The Cl—N distances in these contacts were found in the range 3.252–3.620 Å (3.390 Å on average). The SO_4^{2-} tetrahedron is linked to the cations by 13 NH···O hydrogen bonds with the donor-acceptor distances between 2.819 and 3.043 Å (2.901 Å on average). Although all hydrogen bonds in this crystal structure can be classified as of medium or weak strength, their role in the stabilization of the low-temperature phase III can be prominent. The heating of the crystal to the vicinity of the transition temperature region does not result in significant structural changes, as seen from the data in Table II. At 345 K the ions are still well ordered, but the temperature factors of the atoms are enhanced. Several measurements have been made to collect the data in the narrow temperature range of phase II. The systematic extinctions pointed to the orthorhombic space group $Fmm2$, but the solution of the structure was unsuccessful. The probable reason could be the coexistence of phases and time-evolution of the Bragg intensities during the data collection.

The model of the crystal structure in the high-temperature phase I is shown in Fig. 5(b). In this phase the unit-cell volume halves and the crystals become tetragonal assuming space group $I\bar{4}2m$. The c axis of the tetragonal unit-cell corresponds to the b axis of the orthorhombic phase III. In the tetragonal unit-cell all the ions occupy special positions: the C and N(2) atoms of the G cations are situated on the symmetry planes, the Cl^- ions on the twofold symmetry axes, and the S atoms from the SO_4^{2-} groups are located at the highly symmetric sites of $\bar{4}2m$ symmetry. The tetrahedron symmetry is inconsistent with its site symmetry in the crystal lattice, which imposes disorder of the oxygen atoms. It was established that this disorder was apparently higher than the minimal twofold orientational disorder required by the symmetry of the crystal. It is plausible that the sulfate groups perform rotations about their centers of gravity. In rotating ions the sites of the oxygen atoms are smeared, which was reflected in the refinement process in the anomalous large thermal vibrations of the oxygen atoms along the directions perpendicular to the S—O bonds. Therefore we modeled the orientational disorder of the tetrahedron with partially occupied oxygen sites located around the central S atom. This model agrees well with x-ray diffraction data leading to the low reliability factors as shown in Table I.

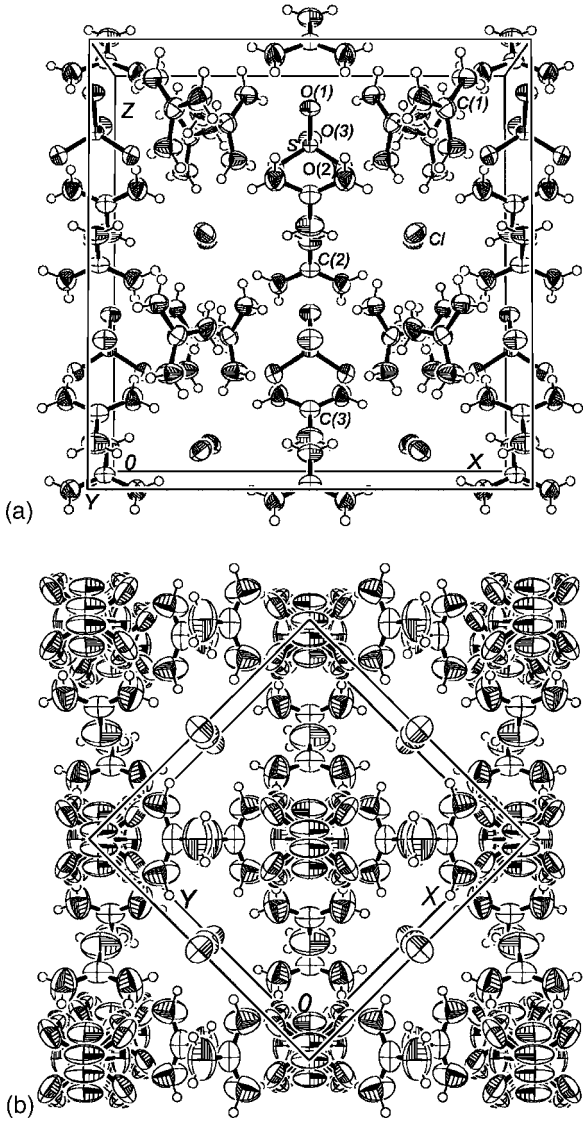

FIG. 5. The $G_4Cl_2SO_4$ crystal structure (a) in the ferroelectric phase III at 298 K viewed along [010] of the orthorhombic unit-cell, and (b) in the paraelectric phase I at 360 K viewed along [001] of the tetragonal unit-cell. To illustrate a relationship between the orthorhombic and tetragonal unit-cells the same orientation of the crystal lattice in both phases has been preserved. For clarity the hydrogen bonds have been omitted. The thermal ellipsoids have been drawn at 50% probability level.

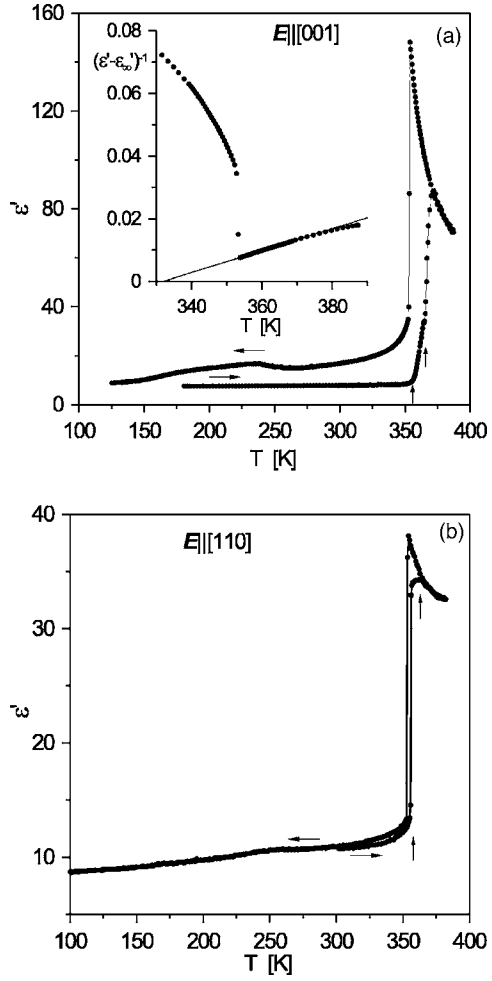

FIG. 6. Temperature dependence of the real part of electric permittivity ε' measured in the first heating-cooling cycle at 10 kHz (a) along [001] and (b) along [110] of the orthorhombic phase III. The vertical arrows mark the transition points. The inset shows the fulfillment of the Curie-Weiss law in the paraelectric phase.

D. Dielectric properties

The symmetry change of the crystal from the polar space group $Cmc2_1$, through the intermediate orthorhombic phase, to the nonpolar one, space group $I\bar{4}2m$, suggests a possible ferroelectric-paraelectric phase transition. This prediction is justified by temperature dependence of electric permittivity shown in Fig. 6. The dielectric constant is anisotropic, especially in the vicinity of the phase transitions. The component measured along [001] of the orthorhombic phase III reaches the maximum value, which is about four times higher than that in the perpendicular direction [110]. On the first heating of the virgin sample two dielectric anomalies, marked with vertical arrows in Fig. 6, have been observed. The first one is manifested as a stepwise increase in ε'. Apparently, in both directions the magnitude of this change is similar and in consequence $\varepsilon' \approx 35$ for both components in the intermediate phase II. Evident differences in the permittivity components are detected at the transition to the high-temperature phase I. While for $\boldsymbol{E}\|[110]$ the anomaly is not very profound, a sharp peak corresponding to the ferroelectric-paraelectric phase transition occurs for the electric field orientation $\boldsymbol{E}\|[001]$. Thus $T_2=T_C$ is a Curie point and the clear anisotropy of dielectric response proves that spontaneous polarization is generated in $G_4Cl_2SO_4$ along [001], consistent with the symmetry of the ferroelectric phase III. On cooling the crystal from the paraelectric phase, only one sharp peak, characteristic of first-order paraelectric-ferroelectric phase transition, was observed. In the paraelectric phase, above T_C, the $\varepsilon'(T)$ dependence obeys the Curie-Weiss law: $\varepsilon'-\varepsilon_\infty=C/(T-T_0)$, where ε_∞ is the high-frequency limit of electric permittivity, C is the Curie-Weiss constant, and T_0 is the Curie-Weiss temperature. The best fitting of the 10 kHz data in the temperature range 354–370 K, as shown in the inset in Fig. 6(a), was obtained with the following parameters: $\varepsilon_\infty=7$, $T_0=328.2$ K, and $C=2860$ K. But it should be stressed that for different crystals we observed a certain scatter in the values of these parameters, as well as the transition temperatures. This effect originates most probably from the crystal imperfections and lattice strains. For example, the Curie-Weiss constant values determined for different samples were within the range of 2600–3400 K.

As seen in Fig. 6(a) the temperature cycling of the crystal through the Curie point results in a remarkable increase of the dielectric constant in the ferroelectric phase. Besides, below 250 K some anomalies, not observed for the virgin samples, have appeared. The dielectric response of the crystal in the low-temperature region is illustrated in Fig. 7. The anomalies in ε' and ε'' are strongly frequency-dependent and their maxima shift to lower temperatures when the frequency of the measuring electric field decreases. Such a behavior is characteristic of dipolar relaxational processes. To analyze the complicated changes in the dielectric functions we plotted ε' and ε'' as a function of $\log(f)$ at different temperatures (Fig. 8). In the temperature range between 255 and 150 K, the loss curves show only one broad and asymmetric peak with full width at half maximum about 2.3 decades, much broader than the 1.14 decades expected for a monodispersive Debye relaxator. This indicates a broad distribution of the relaxation rates, and therefore, we applied a stretched-exponential function of the Kohlrausch-Williams-Watts (KWW) type[23] for modeling the low-temperature dielectric response of the crystal. The complex electric permittivity $\varepsilon(\omega)$ may be written as a Fourier transform of the relaxation function $\Phi(t)$:

$$\frac{\varepsilon(\omega)-\varepsilon_\infty}{\varepsilon_0-\varepsilon_\infty}=1-i\omega\,\Im[\Phi(t)], \tag{1}$$

where ε_0 is a static permittivity, and the KWW function takes the form

$$\Phi(t)=\exp[-(t/\tau)^\beta]. \tag{2}$$

The parameter τ in Eq. (2) represents a characteristic relaxation time and $0<\beta\leqslant 1$ characterizes a distribution of the relaxation times. Equations (1) and (2) were used to fit the ε' and ε'' data. The solid lines in Fig. 8 show the best fit of the KWW function to the experimental points. The β exponents obtained from the fitting procedure varied between 0.43 and 0.53, indicating a broad distribution of the relaxation times.

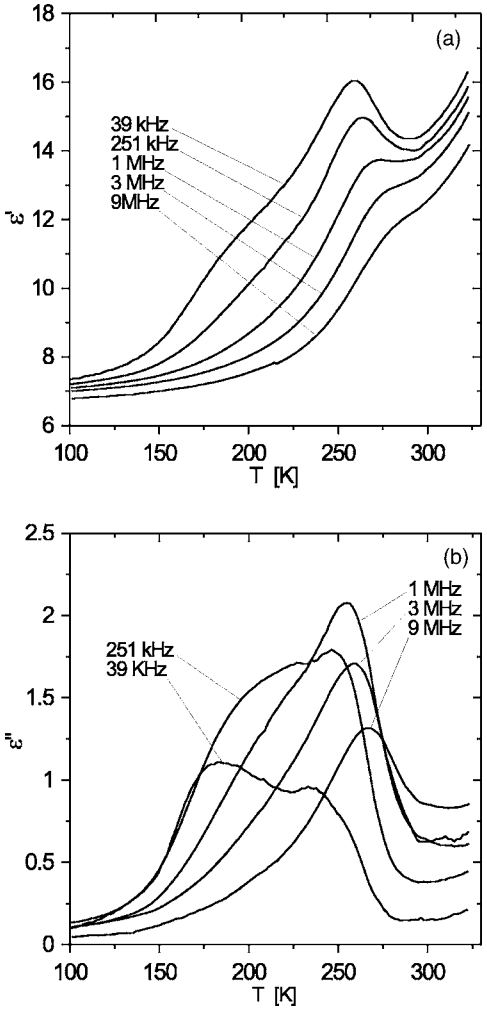

FIG. 7. Temperature and frequency dependencies of the real (a) and imaginary (b) parts of the electric permittivity of $G_4Cl_2SO_4$, measured after the reverse transition of the crystal from the paraelectric phase. The electric measuring field was parallel to the polar direction [001] of the ferroelectric phase III.

The temperature dependence of the τ-values determined using the KWW approach is depicted in Fig. 9. As shown, $\ln(\tau)$ is a linear function of $1/T$, which testifies to the Arrhenius-type behavior. Thus τ obeys the activation relation:

$$\tau = \tau_0 \exp(E_a/k_B T), \tag{3}$$

where τ_0 is a reciprocal of the attempt jump frequency and E_a is the activation energy. The parameters calculated from the fitting are as follows: $E_a = 12.3$ kJ/mol and $\tau_0 = 4.5 \times 10^{-10}$ s.

It should be stressed that the singularities observed in the low-temperature dielectric response of $G_4Cl_2SO_4$ disappeared for the samples kept at room temperature. It is also important that freshly grown crystals exhibited a ferroelectric domain structure [see Fig. 10(a)], but in the frequency range studied the contribution of the ferroelectric domains and domain walls to the complex electric permittivity was rather of minor importance, as clearly seen from the measurements of the virgin crystal (Fig. 6). Obviously, cycling of the crystal

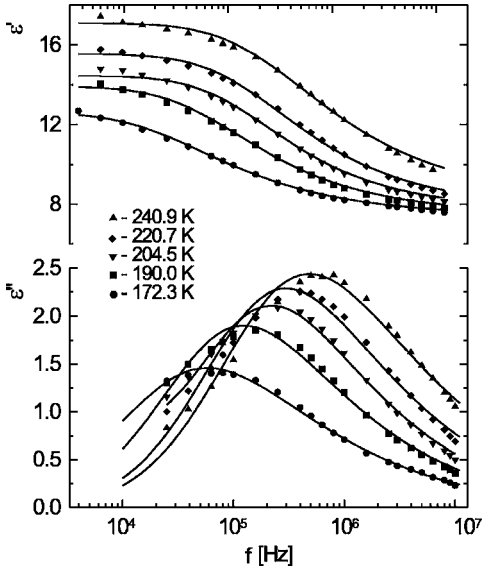

FIG. 8. Frequency dependence of the dielectric functions ε' and ε'' at several temperatures in the ferroelectric phase IV. The solid lines are the fits with the Fourier transform of KWW function.

through T_C resulted in a finer domain pattern, and additionally, the reverse transition from the paraelectric phase produced very fine ferroelastic domain structure, as shown in Fig. 10(b). It was established that ferroelastic domains disappeared at room temperature within a short time, which varied between a few to 20 hours depending on the sample. This process was correlated with the decay of the low-temperature anomalies in dielectric functions.

E. Spontaneous polarization

The clear evidence of ferroelectricity in $G_4Cl_2SO_4$ is provided by the ferroelectric hysteresis loops presented in Fig. 11. The measurements were performed during the heating of the virgin sample [Fig. 11(a)] and subsequent cooling from the paraelectric phase [Fig. 11(b)]. The 50 Hz electric field was applied along the polar direction [001] of the ferroelectric $Cmc2_1$ phase. As seen in Fig. 10(b), at 297 K the hysteresis loop is far away from saturation because of the high coercive field. The coercive field decreases apparently with

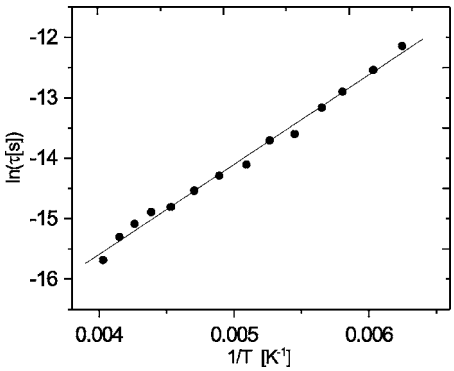

FIG. 9. Arrhenius plot of the characteristic relaxation time derived from the KWW fits.

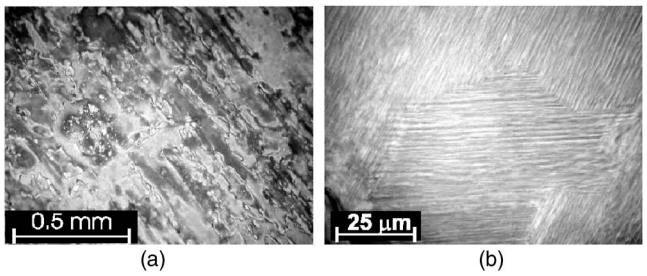

FIG. 10. Ferroelectric domain structure observed in the (010) plane in phase III at 298 K (a); and ferroelastic domains in phase IV at 340 K, observed on the crystal plate oriented perpendicular to the fourfold axis of the tetragonal phase I (b).

increasing temperature, but only in close vicinity of the transition region does the loop starts to resemble the saturated one. At 352 K the spontaneous polarization reaches a value of 2 $\mu C/cm^2$ and the estimated coercive field is still high, about 9.7 kV/cm. In the temperature range between 354 and 362 K a gradual vanishing of the loop was observed, probably due to the coexistence of phases in this temperature region and certain diffuseness of the transitions related to crystal imperfections and internal strains. On cooling the sample, the transition was manifested much more abruptly.

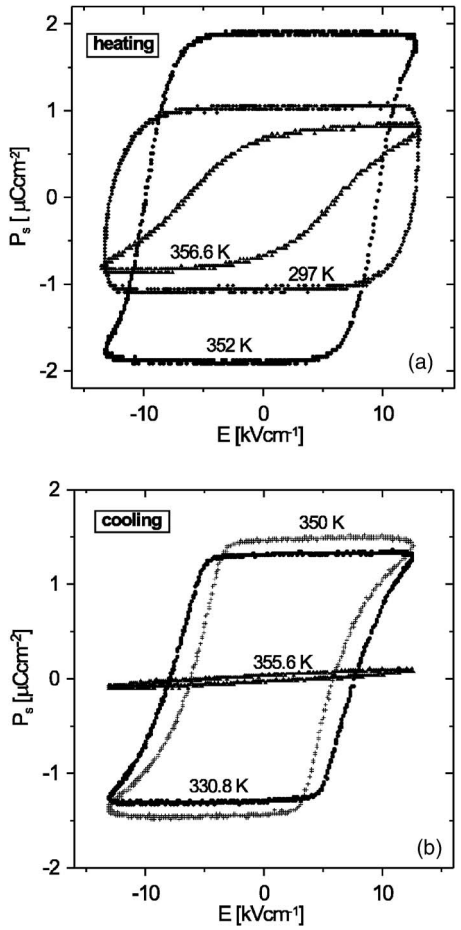

FIG. 11. The hysteresis loops recorded on heating (a) and on cooling (b) the $G_4Cl_2SO_4$ crystal; the 50 Hz electric field was parallel to [001] of the orthorhombic phase III.

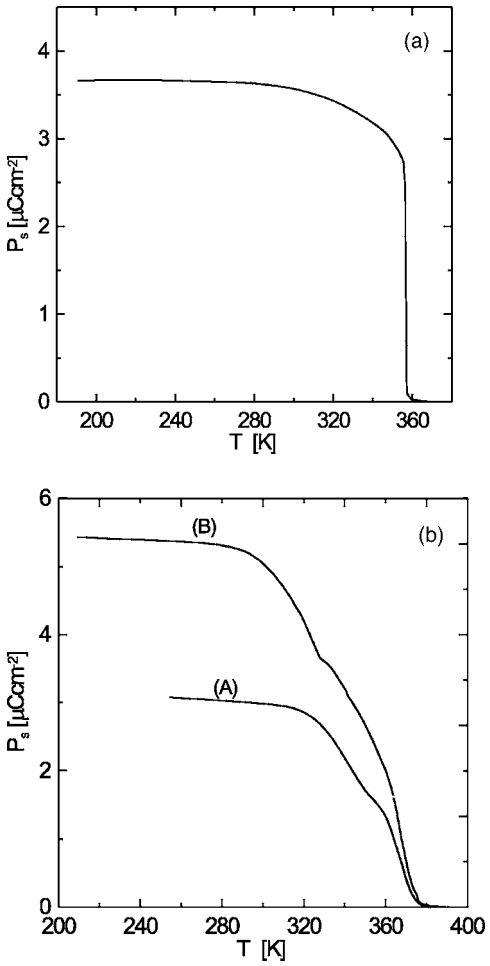

FIG. 12. Temperature dependence of the spontaneous polarization measured by the pyroelectric method in phase IV (a) and in phase III (b), for details see the text.

The hysteresis loop recorded at 350 K [Fig. 11(b)] indicates a coercive field of about 6 kV/cm, that is much reduced when compared to the value observed in the first heating cycle. However, the value of P_s is also reduced to about 1.5 $\mu C/cm^2$. This may be a consequence of defects created in the crystal structure at the transition point, but on the other hand, the reverse transition is accomplished to the low-temperature phase IV, which can be characterized by different P_s than the original ferroelectric phase III.

The spontaneous polarization of the crystal was independently determined from the pyroelectric charge measurements. The crystal was poled while cooling from the paraelectric phase in the dc electric field of 3 kV/cm. Then the pyroelectric charge was measured during the heating of the sample at a temperature rate of 2 K/min. The temperature dependence of P_s determined in this manner is shown in Fig. 12(a). It should be stressed that the magnitude of P_s measured by the pyroelectric method is significantly higher than the value estimated from the hysteresis loop [compare Figs. 12(a) and 11(b). Two reasons should be considered to explain this difference: either the hysteresis loop was still not well-saturated, even in the vicinity of T_C, and hence the lower value of P_s, or the contribution to the pyroelectric

charge from the secondary pyroelectric effect[24] was significant. The other question is the magnitude of P_s in the ferroelectric phase III. From the results presented in Fig. 11 one can conclude that P_s in this phase can be higher then in phase IV. Therefore we have undertaken several attempts to measure spontaneous polarization directly in this phase using the pyroelectric method. For this purpose the crystals had to be poled in phase III without crossing the Curie point. Thus the dc electric field of 10–15 kV/cm (i.e., the highest possible field not leading to the breakdown) was applied to the samples at 345 K and next the crystals were field-cooled. Then after removal of the field, the pyroelectric charge was measured during the heating. The results obtained in this way for different crystals were characterized by a relatively high scatter. This indicates a prominent role of defects in the properties of the "as-grown" $G_4Cl_2SO_4$ crystals. Such defects can cause a pinning of the local polarization, hindering the reversal process during the cycling of the electric field or a transformation of the crystal to the single-domain state. A representative $P_s(T)$ course is shown in Fig. 12(b), curve (A), but it should be stressed that the maximum value of P_s measured in this way varied between 1 and 3 $\mu C/cm^2$. It seems that the electric field applied was not enough to obtain the single-domain crystals and to determine the total value of P_s. Although most of the crystals used in the pyroelectric experiments showed a multidomain ferroelectric structure, similar to that shown in Fig. 10(a), one of the samples tested exhibited almost a single-domain state. The results of pyroelectric measurements on this sample (without the application of the electric poling field) are represented by curve (B) in Fig. 12(b). As seen, in this case we observe the highest value of polarization of about 5.5 $\mu C/cm^2$ at low temperatures, but the temperature dependence of P_s is strongly affected by temperature-induced relaxation of the local strains and lattice imperfections and/or domain structure reconstruction.

IV. DISCUSSION

To elucidate the origin of ferroelectric polarization in $G_4Cl_2SO_4$ we performed a careful analysis of the ferroelectric and paraelectric structures. In phase III the spontaneous polarization occurs along [001] and is mainly a result of the ionic displacements. There are two main factors which determine the total polarization of the crystal. First, the SO_4^{2-} anions are displaced along [001] by 0.267 Å from their symmetric sites with respect to the Cl^- neighbors. Second, there are 16 guanidinium cations in the unit cell, which occupy three different sites. Namely, there are eight $G(1)$, four $G(2)$ and four $G(3)$ cations. The three crystallographically different cations are displaced in different ways with respect to both anionic sublattices. These displacements are indicated by the thin arrows in Fig. 13. Assuming point charges on the ionic central atoms, the value of $\boldsymbol{P_s}$ was calculated from the ionic displacements. As shown in Fig. 13, the $\boldsymbol{P_2}$ and $\boldsymbol{P_3}$ vectors have the opposite senses and therefore the contributions of the $G(2)$- and $G(3)$-type cations are partially cancelled, giving rise to the resultant component of the same sense as $\boldsymbol{P_1}$. The summing up of all contributions gave the value of 11.02 $\mu C/cm^2$ for the total spontaneous polarization of the crystal at 298 K. Similar calculations were made using the structural data collected at 345 K. At this temperature the value of $\boldsymbol{P_s}$ derived from the model amounts to 10.46 $\mu C/cm^2$. Thus this simple point-charge approximation quite reasonably reproduces the temperature behavior of $\boldsymbol{P_s}$, and more important still, the model explains the displacive

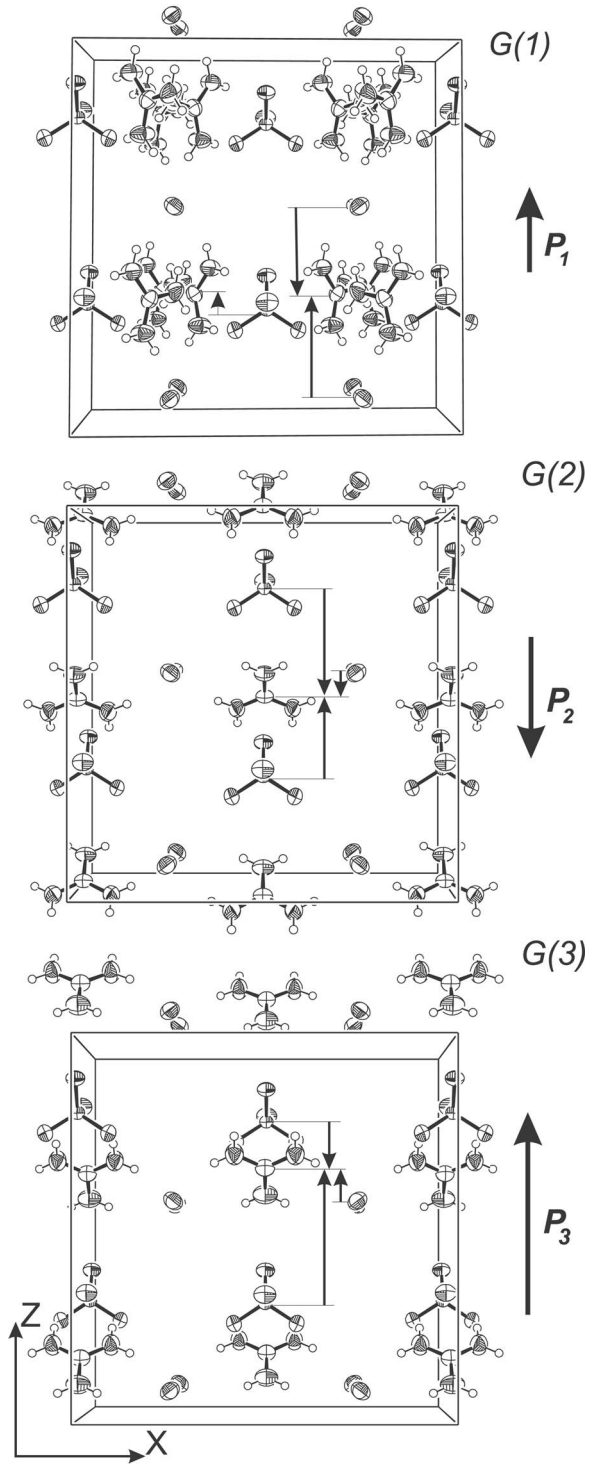

FIG. 13. Schematic illustration of the contributions to the total polarization of the crystal. The displacements of the three crystallographically different guanidinium cations with respect to the Cl^- and SO_4^{2-} anions are shown with thin arrows.

nature of ferroelectricity in $G_4Cl_2SO_4$. Although it seems that the magnitude of polarization may be overestimated due to the effects which were not taken into account. Additional contributions to spontaneous polarization may arise from the molecular dipoles induced by slight distortions of the ionic geometries in the crystal lattice, and charge distribution along the hydrogen bonds.

The clearly displacive character of spontaneous polarization does not contradict an order-disorder mechanism of the transitions in $G_4Cl_2SO_4$. The order-disorder contribution is evident from the high value of the transition entropy and structural models of the para- and ferroelectric phases. The triggering of the rotations of the SO_4^{2-} tetrahedron results in an averaging of its interactions with neighboring ions, which makes that the Cl^- and SO_4^{2-} anions assume equidistant sites in the tetragonal phase and the arrangement of the structure becomes more symmetric. Thus dynamical disorder drives the phase transitions leading to the vanishing of $\boldsymbol{P_s}$ in the paraelectric phase. However, it should be noted that the multiconfigurational disorder of the SO_4^{2-} tetrahedrons may not be sufficient to explain the total entropy change associated with the transitions at 352 and 356 K. The additional contribution to the transition entropy can arise from the disorder of the cations. Although such a disorder was not directly evidenced by the structural data, the nitrogen atoms of the *G* cations exhibit much more enhanced thermal ellipsoids in the paraelectric phase, at 360 K, when compared to those at 345 K. Therefore it cannot be excluded that the cations are split, but with relatively small angles between the equivalent orientations. This type of disorder is rather difficult to detect by standard crystallographic methods.[25]

It is also worth noting that the transition to the paraelectric phase is associated with a negative change in the crystal volume (see Fig. 3). Thus the crystal structure is more tightly packed above T_C than below this temperature. The contraction of the crystal at T_C implies a negative pressure coefficient dT_C/dp, which is characteristic of displacive-type ferroelectric phase transitions.[27]

The behavior of the $G_4Cl_2SO_4$ crystals on cooling from the paraelectric phase pertain to the most unusual. The paraelectric-ferroelectric phase transition is accomplished between the tetragonal phase I and phase IV of the symmetry lower than that of the initial orthorhombic phase III. The latter conclusion is derived from the observations of the ferroelastic domain structure. The symmetry change from tetragonal to orthorhombic would result in 90° domain walls between the possible orientational states.[26] As seen in Fig. 10(b), it is clearly not the case. The domain pattern observed indicates that the crystal symmetry in phase IV can be monoclinic or triclinic. It is prominent that this phase is thermodynamically metastable and its structure must be highly disordered, according to the results of calorimetric studies. The plausible explanation may be as follows. The prevailing part of the orientational degrees of freedom of dynamically disordered ions in the paraelectric phase is frozen below T_C in a static or a very long relaxation-time state. At room temperature, due to the structural relaxation processes, the crystal transforms slowly to the ordered phase, which is most probably the orthorhombic phase III. Full crystallization requires about 2 weeks. Much faster changes were observed in the ferroelastic domain pattern of the crystals kept at room temperature. The decay time of the domain pattern was similar as the time of disappearing of the low-temperature anomalies in dielectric functions. This correlation indicates that the relaxational processes observed in $G_4Cl_2SO_4$ originates from the fine ferroelastic domain structure rather than from the structural relaxation of the metastable phase IV.

V. CONCLUSIONS

It has been demonstrated that the crystal of $G_4Cl_2SO_4$, a synthesized compound from the guanidinium salts group, exhibits ferroelectric properties at room temperature, similarly as the well-known GASH. But it is different from the GASH-type ferroelectrics owing to the presence of the Curie-point. The spontaneous polarization of 3.6 $\mu C/cm^2$, derived from the pyroelectric-charge measurements in phase IV, is the same as reported for GASH at room temperature.[1] However, the experiments performed in the ferroelectric phase III indicate that P_s may be even higher than 5.5 $\mu C/cm^2$. The high value of P_s is also predicted by the model calculations based on the point-charge approximation and the crystal structure in the orthorhombic $Cmc2_1$ phase. Unfortunately, a precise determination of the net value of P_s in phase III failed due to the high coercive field, exceeding 15 kV/cm at room temperature. This high value of the coercive field is related to the displacive mechanism of P_s generation, which involves the relative displacements of the anionic sublattices built of the monovalent Cl^- and divalent SO_4^{2-} ions, and the displacements of the guanidinium cations from their high-symmetry sites in the tetragonal phase. Thus there are several contributions to P_s associated with profound changes in the crystal structure, which can be characterized by different susceptibilities to the reversal processes. The reversal of P_s in $G_4Cl_2SO_4$ seems to be also strongly dependent on the density of lattice defects and the related aging phenomena.

Of particular interest is the phase diagram of this ferroelectric crystal. At ambient pressure the phase relations can be summarized as follows:

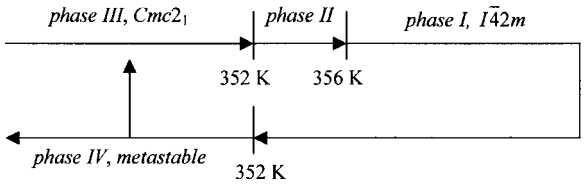

Thus, in the temperature range below T_C, the crystal can exist in the ordered ferroelectric phase III or in the disordered ferroelectric phase IV, which shows metastable features. The nature of such a behavior of the crystal requires further studies.

ACKNOWLEDGMENT

The author is grateful to Professor Andrzej Katrusiak of the Department of Chemistry, Adam Mickiewicz University, for valuable discussions.

[1] A. N. Holden, B. T. Matthias, W. J. Merz, and J. P. Remeika, Phys. Rev. **98**, 546 (1955).
[2] C. L. Angell, N. Sheppard, A. Yamaguchi, T. Shimanouchi, T. Miyazawa, and S. Mizushima, Trans. Faraday Soc. **53**, 589 (1957).
[3] V. A. Russell, M. C. Etter, and M. D. Ward, J. Am. Chem. Soc. **116**, 1941 (1994).
[4] V. A. Russell, C. C. Evans, W. Li, and M. D. Ward, Science **276**, 575 (1997).
[5] J. A. Swift, A. M. Pivovar, A. M. Reynolds, and M. D. Ward, J. Am. Chem. Soc. **120**, 5887 (1998).
[6] Z. Pająk, M. Grottel, and A. E. Kozioł, J. Chem. Soc., Faraday Trans. 2 **78**, 1529 (1982).
[7] A. Katrusiak and M. Szafrański, Acta Crystallogr., Sect. C: Cryst. Struct. Commun. **C50**, 1161 (1994).
[8] A. Katrusiak and M. Szafrański, J. Mol. Struct. **378**, 205 (1996).
[9] M. Szafrański, Solid State Commun. **84**, 1051 (1992).
[10] M. Szafrański and A. Katrusiak, Chem. Phys. Lett. **391**, 267 (2004).
[11] M. Szafrański and A. Katrusiak, Phys. Rev. B **61**, 1026 (2000).
[12] R. Jakubas, J. Zaleski, B. Kosturek, and G. Bator, J. Phys.: Condens. Matter **11**, 4731 (1999).
[13] R. Jakubas, P. Ciąpała, A. Pietraszko, J. Zaleski, and J. Kusz, J. Phys. Chem. Solids **59**, 1309 (1998).
[14] M. Szafrański, Thermochim. Acta **307**, 177 (1997).
[15] F. Jona and G. Shirane, *Ferroelectric Crystals* (Dover, New York, 1993).
[16] D. J. Haas, D. R. Harris, and H. H. Mills, Acta Crystallogr. **19**, 676 (1965).
[17] M. Grottel and Z. Pająk, J. Chem. Soc., Faraday Trans. 2 **80**, 553 (1984).
[18] S. Gima, Y. Furukawa, and D. Nakamura, Ber. Bunsenges. Phys. Chem. **88**, 939 (1984).
[19] P. Dera, A. Katrusiak, and M. Szafrański, Pol. J. Chem. **74**, 1637 (2000).
[20] H. Diamant, K. Drenck, and R. Pepinsky, Rev. Sci. Instrum. **22**, 30 (1957).
[21] G. M. Sheldrick, SHELXS97, program for solution of crystal structures, University of Göttingen, Göttingen, 1997.
[22] G. M. Sheldrick, SHELXL97, program for crystal structure refinement, University of Göttingen, Göttingen, 1997.
[23] G. Williams and D. C. Watts, Trans. Faraday Soc. **66**, 80 (1970).
[24] J. F. Nye, *Physical Properties of Crystals. Their Representation by Tensors and Matrices* (Clarendon, Oxford, 1957).
[25] R. Rohleder, T. Luty, and B. Kuchta, J. Chem. Phys. **100**, 1573 (1994).
[26] J. Sapriel, Phys. Rev. B **12**, 5128 (1975).
[27] G. A. Samara, J. Phys. Soc. Jpn. **28**, 399 (1969).